Nuclear Instruments and Methods in Physics Research A260 (1987) 381–402
North-Holland, Amsterdam

THE RESOLUTION FUNCTION OF A PULSED-SOURCE NEUTRON CHOPPER SPECTROMETER

C.-K. LOONG, S. IKEDA * and J.M. CARPENTER

Argonne National Laboratory, Argonne, Illinois 60439, USA

Received 3 November 1986 and in revised form 12 March 1987

We introduce a formulation for the evaluation of the incident neutron intensity distribution for a chopper time-of-flight spectrometer at a pulsed neutron source. This treatment, incorporated with an assumed scattering function of the sample and the detector geometry, enables calculations of the shape of the time-of-flight intensity profiles of the incident and the scattered neutrons sensed by a neutron detector, thus providing direct comparison with experimental results. The resolution function, $R(Q, E)$, is calculated for a nondispersive scatterer at a resonant energy E. The results of the calculations on the basis of this theory are substantiated by measured spectra obtained by the two chopper spectrometers, HRMECS and LRMECS, at the Argonne Intense Pulsed Neutron Source under a variety of experimental conditions. In all cases we find excellent agreement between calculations and experiments. Using these results we present a procedure for the determination of the mean incident neutron energy and the calibration of the energy-transfer scale for pulsed-source chopper spectrometers. These latter do not follow accurately from simple analysis, and are the main objects of this paper.

1. Introduction

The goal of a neutron scattering experiment is to determine the scattering function, $S(\boldsymbol{Q}, E)$ where $\boldsymbol{Q}$ and E are respectively the neutron momentum and energy transfer, from which one obtains information on the intrinsic structure and dynamics of the system being studied. In practice one measures a quantity which is a convolution integral given by

$$I_s(\boldsymbol{Q}, E) = \int\int R(\boldsymbol{Q}' - \boldsymbol{Q}, E' - E) S(\boldsymbol{Q}', E')\, \mathrm{d}\boldsymbol{Q}'\, \mathrm{d}E'. \tag{1}$$

In the above expression $R(\boldsymbol{Q}' - \boldsymbol{Q}, E' - E)$ is the instrumental resolution function which defines the probability of detecting a neutron as a function of $\Delta\boldsymbol{Q}(= \boldsymbol{Q}' - \boldsymbol{Q})$ and $\Delta E(= E' - E)$ when the instrument is set to measure the scattering processes at $(\boldsymbol{Q}, E)$. Clearly, from the experimental point of view, it is important to understand and to optimize this function so as to extract quantitative information on $S(\boldsymbol{Q}, E)$.

The resolution function of neutron time-of-flight chopper spectrometers has been studied by a number of workers [1–6]. In the case of the double-rotor spectrometer at steady-state reactor sources, the shape of a pulse transmitted through the curved, multiple-slit packages of two phased Fermi choppers has been examined [1,2,7]. Analytical expressions of the uncertainties in time as the pulse propagates through various components of the instrument can be derived. The overall uncertainty is then obtained by summing these terms in quadrature. In normal situations the resolution function can adequately be described by a Gaussian function. Another approach is to simulate the generation, the propagation, the scattering processes by the sample and detection of neutrons by a Monte Carlo method. This technique [8,9] has been applied successfully to assess the effects of instrumental resolution and multiple scattering in the sample in a neutron scattering experiment.

Recently, the advent of pulsed spallation neutron sources has aroused the employment and development of chopper spectrometers in a variety of disciplines of condensed matter research. First, these sources

* Permanent address: National Laboratory for High Energy Physics, Oho-machi, 305 Ibaraki-ken, Japan.

have an intense, undermoderated spectral component of epithermal neutrons. When cold moderators are installed, they can provide high fluxes of neutrons with energies ranging from about 1 meV to 10 eV. Second, because of the relatively short pulse widths, time-of-flight techniques are well suited and can be applied with high efficiency. Only one rotor phased with the pulsed source is sufficient to produce neutron bursts with velocities in a narrow range. The neutron pulses emerging from the moderator of a pulsed source, on the other hand, in general have complex time and velocity structures characterized by the target–moderator system. We find that considerations of the resolution function for double-rotor spectrometers at reactors such as the Gaussian approximation are no longer adequate. Moreover, to the best of our knowledge the procedure for the calibration of an energy-transfer scale from experimental data for a pulsed-source chopper instrument has not been rigorously considered before. In this paper we describe the formulation of the resolution function for a pulsed-source chopper spectrometer and the application of this computation in instrumental calibration and data analysis at the Intense Pulsed Neutron Source (IPNS) of Argonne National Laboratory.

The plan of this paper is as follows: In sect. 2, we first introduce the formulation of the resolution calculation and then outline the analytical functions for the description of the important components in a pulsed-source chopper spectrometer and discuss the associated effects on resolution. Since we find good agreement between calculations and experimental data obtained by the two chopper spectrometers at IPNS, we give a brief description of the characteristics of the IPNS target–moderator system and the spectrometer parameters in sect. 3. In sect. 4 we discuss the application of the resolution calculations and compare the results with experimental data.

2. Formulation of the resolution calculation

Since the details of the IPNS chopper spectrometers have been given elsewhere [10], we describe only briefly the operation here. Fig. 1 shows the schematic layout of the two chopper spectrometers at IPNS. Pulses of medium energy ($\sim$ 500 MeV) protons impinging on a heavy metal (e.g., uranium) target generate intense pulses of neutrons. These neutrons are moderated by the moderator made of hydrogenous materials and then emerge from the surface with repetition frequency ν. A Fermi chopper rotating at a mean angular frequency a multiple of ν is located at a distance l_1 from the moderator surface. By maintaining the chopper in a fixed phase relation to the proton pulses only neutrons within a narrow velocity range are transmitted through the chopper window. A Soller slit collimator downstream of the

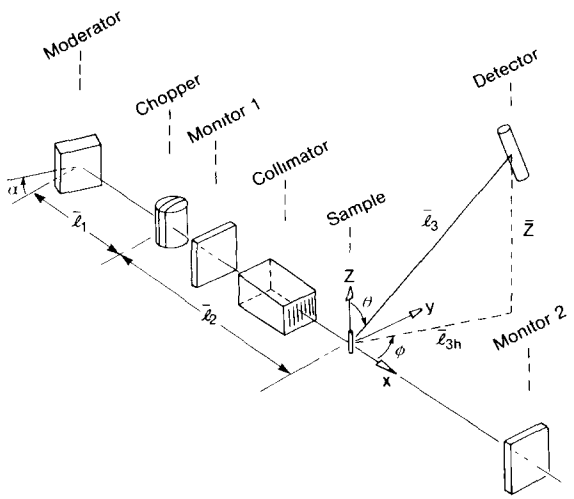

Fig. 1. The schematic layout of the chopper spectrometers at IPNS.

chopper refines the horizontal divergence of the neutron bursts before they are incident on the sample. The intensity of the scattered neutrons is recorded as a function of time of flight, t, by over two hundred ^{3}He proportional counters centered at positions defined by $(\bar{l}_3, \bar{\phi}, \bar{\theta})$, where $\bar{l}_3$, $\bar{\phi}$, and $\bar{\theta}$ are the mean distance between sample and a detector element, the mean scattering and the azimuthal angle respectively. Two low-efficiency BF_3 fission detectors placed in the direct beam monitor the intensity and energy of the incident neutrons.

Consider that a neutron takes a flight time t_1 to travel from the emission point on the moderator face to the center of the chopper at a distance l_1 away. The incident velocity is simply

$$v_i = l_1/t_1. \tag{2}$$

If the neutron impinges on a sample at l_2 downstream from the chopper and is scattered to (l_3, ϕ, θ) at time t, then the final neutron speed is

$$v_f = \frac{l_3}{t - t_s}, \tag{3}$$

where l_3 is the distance between the sample and the point of detection and t_s the arrival time at the sample. Correspondingly to eq. (2),

$$t_s = \frac{l_1 + l_2}{v_i}. \tag{4}$$

The neutron energy and momentum transfer are, respectively,

$$E = \frac{m}{2}\left(v_i^2 - v_f^2\right), \tag{5}$$

$$\boldsymbol{Q} = \frac{m}{\hbar}(\boldsymbol{v}_i - \boldsymbol{v}_f). \tag{6}$$

where m is the mass of the neutron. In the coordinate system shown in fig. 1,

$$Q_x = \frac{m}{\hbar}(v_i - v_f \sin\theta \cos\phi), \tag{7a}$$

$$Q_y = -\frac{m}{\hbar} v_f \sin\theta \sin\phi, \tag{7b}$$

$$Q_z = -\frac{m}{\hbar} v_f \cos\phi. \tag{7c}$$

Considering the spectrometer measuring an effective $(\boldsymbol{Q}, E)$ transfer from the observed intensity at the corresponding final flight time, there exist uncertainties in time due to the source pulse width, the chopper opening time, as well as ambiguities in the incident and scattered flight distances due to the moderator geometry, chopper and collimator window dimensions, and the sample and detector sizes. The velocity spreads of the incident and scattered neutrons are defined respectively by the chopper and the scattering function and are constant throughout the flight path. The time spreads, on the other hand, propagate according to the velocity and the distance of travel. Therefore, in order to fully account for these effects, we need to consider in a general fashion the observed intensity at a mean position $\bar{\boldsymbol{r}} = (\bar{l}_3, \bar{\phi}, \bar{\theta})$ as a function of neutron speed v and flight time t. First, let us consider the incident intensity as a function of neutron velocity and time-of-flight at a distance l downstream of the chopper. This is given by

$$\begin{aligned} I_0(v, t) &= \Phi_0(v)\eta(v)\int\int\int\int\int \mathrm{d}t_p\, \mathrm{d}t_1\, \mathrm{d}t_0\, \mathrm{d}l_1\, \mathrm{d}lP(v, t_p)W(t_1 - t_0)\zeta_{l_1}\zeta_l \\ &\quad \times\delta(t_1 - t_p - l_1/v)\ \delta(t - t_p - l_1/v - l/v) \\ &= \Phi_0(v)\eta(v)\int\int\int \mathrm{d}t_0\, \mathrm{d}l_1\, \mathrm{d}lP(v, t - l_1/v - l/v)W(t - l/v - t_0)\zeta_{l_1}\zeta_l \\ &= \Phi_0(v)\eta(v)\int \mathrm{d}li(v, t - l/v)\zeta_l \\ &\equiv G(v, t - \bar{l}/v), \end{aligned} \tag{8}$$

where

$$i(v, u) = \int \mathrm{d}t_0 \, \mathrm{d}l_1 \, P(v, u - l_1/v) W(u - t_0) \zeta_{l_1}. \tag{9}$$

In the above equations, t_p t_1 and t_0 are the emission time on the moderator face, the arrival time at the chopper center and the chopper open time with respect to the time origin respectively; P, W, Φ_0 and η are the functions for the primary source pulse, the chopper–collimator system, the incident spectrum and the detector efficiency respectively. ζ_x is the probability distribution function for the variable x, and $\bar{l}$ is the mean of distance l. We have assumed that the pulse function varies independently in v and t_p so that Φ_0 can be written as a prefactor in eq. (8). In an experiment, a beam monitor senses all the transmitted neutrons with different velocities. Therefore, the observed intensity profile is

$$I_0(t) = \int \mathrm{d}v \, i(v, t), \tag{10}$$

and the mean time of flight for the incident neutrons measured by a monitor detector located at a mean distance $\bar{l}$ downstream of the chopper is

$$\bar{t}_l \equiv \int \mathrm{d}t \, t I_0(t) \int \mathrm{d}t \, I_0(t). \tag{11}$$

The velocity distribution of neutrons transmitted through the chopper is

$$J_0(v) \equiv \int \mathrm{d}t \, i(v, t), \tag{12}$$

and the mean incident neutron speed and energy are, respectively,

$$\bar{v}_1 \equiv \int \mathrm{d}v \, v J_0(v) \int \mathrm{d}v J_0(v), \tag{13a}$$

and we take

$$\bar{E}_1 \equiv \frac{m}{2} \bar{v}_1^2. \tag{13b}$$

Now suppose that a neutron is scattered by the sample to a detector and the scattering processes are governed by a scattering function $S(\boldsymbol{Q}, E)$ and by eqs. (5) and (6). The scattered intensity can be written as

$$\begin{aligned} I_s(\boldsymbol{Q}, E, t) = & \int\int\int\int\int\int\int \mathrm{d}E' \, \mathrm{d}\boldsymbol{Q}' \, \mathrm{d}v_1 \, \mathrm{d}v_f \, \mathrm{d}t_s \, \mathrm{d}l_s \, \mathrm{d}l_3 \, i(v_1, t_s)(v_f/v_1)\eta(v_f) \\ & \times S(\boldsymbol{Q}', E') \zeta_{l_s} \zeta_{l_3} \delta(t - t_s - l_3/v_f) \delta(E' - E) \delta\left(Q' - \sqrt{\frac{m^2}{\hbar^2}(v_1^2 + v_f^2 - 2\boldsymbol{v}_1 \cdot \boldsymbol{v}_f)} \right) \\ \equiv & \int\int \mathrm{d}E' \, \mathrm{d}\boldsymbol{Q}' \, R(\boldsymbol{Q}' - \boldsymbol{Q}, E' - E, t) S(\boldsymbol{Q}', E'), \end{aligned} \tag{14}$$

where R is the resolution function. In particular, if (as for a nondispersive scatterer)

$$S(\boldsymbol{Q}, E) = \delta(E - \epsilon), \tag{15a}$$

then

$$\begin{aligned} I_s(\epsilon, t) = & R(\epsilon, t) \\ = & \int\int\int\int\int\int \mathrm{d}E' \, \mathrm{d}v_1 \, \mathrm{d}v_f \, \mathrm{d}t_s \, \mathrm{d}l_s \, \mathrm{d}l_3 \, i(v_1, t_s)(v_f/v_1)\eta(v_f) \\ & \times \zeta_{l_s} \zeta_{l_3} \delta(t - t_s - l_3/v_f) \delta(E' - \epsilon). \end{aligned} \tag{15b}$$

Therefore, when the spectrometer is set to measure the scattering processes at $(\boldsymbol{Q}, E)$, the variance in time-of-flight is given by

$$\sigma_t^2 = \frac{\int \mathrm{d}t(t-\bar{t}_3)^2 I_s(\boldsymbol{Q}, E, t)}{\int \mathrm{d}t I_s(\boldsymbol{Q}, E, t)}, \tag{16a}$$

where we take

$$\bar{t}_3 = \bar{t}_s + \frac{\bar{l}_3}{\sqrt{\bar{v}_1^2 - 2E/m}}. \tag{16b}$$

The standard deviations of the energy and momentum transfer, δE and δQ, are respectively given by

$$\sigma_E = \bar{E}_f\left(\frac{2\sigma_t}{\bar{t}_3 - \bar{t}_s}\right), \tag{17a}$$

$$\sigma_Q^2 = \frac{\int \mathrm{d}t(\boldsymbol{Q}-\bar{\boldsymbol{Q}})^2 I_s(\boldsymbol{Q}, E, t)}{\int \mathrm{d}t I_s(\boldsymbol{Q}, E, t)}. \tag{17b}$$

where $\bar{\boldsymbol{Q}}$ is the mean momentum transfer defined by E, $\bar{v}_1$ and the detector mean position and the integrals in eq. (17b) are performed over a time interval centered at $\bar{t}_3$ corresponding to a resolution element. As an approximation, we compute the fwhms of the energy and momentum transfer distributions as though for Gaussian distributions

$$\Delta E = \sqrt{8 \ln 2}\,\sigma_E, \tag{18a}$$

and

$$\Delta Q = \sqrt{8 \ln 2}\,\sigma_Q. \tag{18b}$$

Now we describe the various functions for the source pulse shape, the chopper, collimator, etc. which are required for the calculation of the resolution function.

2.1. The incident neutron spectrum

For pulsed neutron sources, requirements of high flux but narrow pulses have led to complex designs [4] of the target–moderator system. This involves the optimal configuration of the target, moderator and reflector assembly, a judicious choice of moderator materials and operation temperature, deliberate addition of neutron absorbers around and inside the moderators, etc. The spectral and pulse characteristics of the IPNS ambient temperature polyethylene and low-temperature methane moderators and the radiation-induced effects have recently been studied by Carpenter et al. [11]. We have adopted the spectral function introduced by these authors since it describes very well the incident beam spectra obtained by the monitor detectors at IPNS. It can be written using a modified form of Westcott's function, which joins the Maxwellian component at thermal energies and the "slowing-down" component in the epithermal region, as follows:

$$\Phi_0(E) = \Phi_{\mathrm{MB}}(E) + \Phi_{\mathrm{SD}}(E), \tag{19}$$

where

$$\Phi_{MB}(E) = \Phi_{Th}\frac{E}{E_T^2}\exp\left(-\frac{E}{E_T}\right), \tag{20a}$$

$$\Phi_{SD}(E) = \frac{\Phi_{epi}}{E}\left[1+\left(\frac{E_{co}}{E}\right)^{s}\right]^{-1}\left(\frac{E}{E_{ref}}\right)^{\xi}. \tag{20b}$$

In the Maxwellian part Φ_{MB}, $E_T = k_B T_{ref}$ is the mean thermal energy, related to the effective temperature T_{eff}, which is usually somewhat above the physical temperature of the moderator. Φ_{Th} is the integrated Maxwellian flux. In the slowing-down part Φ_{SD}, the second factor in eq. (20b) is the "joining function" in which E_{co} is the cutoff energy about five times the thermal energy E_T and s is a parameter. The last factor represents the effect of leakage from the moderator medium; ξ is the "leakage exponent" and $E_{ref} = 1000$ meV, Φ_{epi} is the epithermal flux. Fitting eq. (20) with observed data usually gives a normalized χ^2 less than 2.0.

2.2. The pulse-shape function

Knowledge of the emission time distribution of the source pulse (pulse shapes) over a wide range of neutron energies is essential for the analysis of instrumental resolution. Several workers [12–14] have used different functions for pulse shape analysis before. Recently Ikeda and Carpenter [14] introduced a novel function which fits very well the time structure of neutron pulses from the IPNS ambient-temperature polyethylene moderators over an energy range from about 2.5 meV to 1.0 eV. Our experience showed that this function, with a new set of parameters, can also describe the pulse shapes of the IPNS low-temperature methane moderators. This function [14] can be written as

$$P(v, t) = (1-R)(at)^2\exp(-at) + \frac{Ra^2b}{(a-b)^3}\left\{2\exp(-bt) - \left[2+2(a-b)t+(a+b)^2t^2\right]\exp(-at)\right\}, \tag{21}$$

for $t > 0$,

where the first term (slowing-down term) corresponds to the time distribution of neutrons which emerge in the process of slowing down in an infinite, absorption-free medium of free protons before thermalization and the second term (storage term) represents the time decay of the neutrons which emerge after thermalization in the moderator. a ($\simeq \Sigma v$ where Σ is the macroscopic neutron scattering cross section of the moderator) and b (energy independent) are the inverse time constants for the above processes. R is the ratio of the storage and the slowing-down components and can be expressed in terms of a Boltzman function as

$$R = \exp(-E/E_0), \tag{22}$$

where E is the neutron energy and $E_0 \simeq 5k_B T_{mod}$ (T_{mod} is the physical temperature of the moderator).

2.3. Chopper window function

The time uncertainty associated with a Fermi rotor phased with the source involves the time spread defined by the rotor slits and the scan time of the rotor window sweeping across the moderator face (the "lighthouse" effect). We write

$$\Lambda_r(t') = \Lambda_s * \Lambda_m, \tag{23}$$

where $t' \equiv t_1 - t_0$ is the difference in time between the arrival time at the chopper center and the mean chopper open time, $\Lambda_s * \Lambda_m$ is the convolution of the window functions for a single slit of the rotor in a parallel beam and for the lighthouse effect.

The rotor slit transmission has been considered extensively by several authors [1,7]. Here we use a triangular function approximately (variance preserved) describing of the pulse formed by a single, curved, parallel-sided slit of perfectly absorbing material, chopping a perfectly collimated beam [15]:

$$\Lambda_s(t') = \left(1 - \frac{|t'|}{\Gamma_s}\right)\Theta\left(1 - \frac{|t'|}{\Gamma_s}\right), \tag{24}$$

where

$$\Gamma_s = \sqrt{6}\,\frac{d}{2r\omega}\,\sigma_\chi(\beta), \tag{25}$$

$$\sigma_\chi^2(\beta) = \begin{cases} \dfrac{1}{10}\left(\dfrac{5 - 128\beta^4}{3 - 8\beta^2}\right), & \text{for } 0 \le \beta \le \frac{1}{4}, \\ \frac{8}{5}\left(\sqrt{\beta} - \beta\right)^2\left(\dfrac{4 + \sqrt{\beta}}{2 + \sqrt{\beta}}\right), & \text{for } \frac{1}{4} < \beta \le 1, \\ \text{undefined}, & \text{for } \beta > 1, \end{cases} \tag{26}$$

$$\beta \equiv \frac{r^2\omega}{d}\left(\frac{1}{v_{\text{opt}}} - \frac{1}{v}\right), \tag{27}$$

$$v_{\text{opt}} = 2\rho\omega. \tag{28}$$

Here $\Theta(x - x_0)$ is Heaviside's unit function, r is the rotor radius, ω the rotor angular speed, ρ the slit curvature radius and d the slit with. In reality the chopper slats are not made of completely neutron-opaque materials; therefore, neutrons of energies different from the chosen energy may transmit through the rotor window. This chopper "grey edge" effect may result in a transmission somewhat different from the idealized function given by eq. (24). We have investigated this effect by Monte Carlo computer simulation [16] of the neutron transmission probability through slit packages made of materials with effective neutron scattering cross sections corresponding to the IPNS rotors. We find that the grey edge effect is negligible for the IPNS rotors for neutrons of energy up to about 1 eV.

The time broadening due to the chopper lighthouse effect depends on the widths of moderator face and chopper window, the chopper angular speed, and the horizontal angle subtending the moderator face from the chopper center. The corresponding window function Λ_m can be expressed as a trapezoidal function characterized by Γ_1 (and Γ_2), which is the time at which the chopper window lower (and upper) edge sweeps the lower edge of the moderator face relative to the chopper mean open time at which the center line of the chopper window coincides with the center line of the moderator face.

If $2h$ is the width of the cross sectional area of the moderator normal to the beam direction and $2w_r$ is the width of the chopper slit package, then

$$\Gamma_1 = \frac{\gamma - \delta}{\omega}, \tag{29a}$$

$$\Gamma_2 = \frac{\gamma + \delta}{\omega}, \tag{29b}$$

where

$$\gamma = \tan^{-1}\left(h/\bar{l}_1\right) \approx h/\bar{l}_1, \tag{29c}$$

$$\delta = \sin^{-1}\left(\frac{w_r}{\sqrt{\bar{l}_1^2 + h^2}}\right) \approx w_r/\bar{l}_1, \tag{29d}$$

and assuming $\Gamma_1 > 0$ (the usual case, i.e., $h > w_r$)

$$\Lambda_m(t') = \begin{cases} 1, & \text{for } |t'| < \Gamma_1, \\ 1 - A(|t'| - \Gamma_2), & \text{for } \Gamma_1 \leqslant |t'| \leqslant \Gamma_2, \\ 0, & \text{for } |t'| > \Gamma_2, \end{cases} \tag{30}$$

with

$$A \equiv \frac{1}{\Gamma_2 - \Gamma_1} > 0. \tag{31}$$

2.4. Correction of l_1 due to moderator tilt

As the rotor sweeps across the moderator face whose normal is at an angle α relative to the beam direction (see fig. 1), the instantaneous average distance between the emission point on the moderator face to the center of the rotor varies from the mean distance between the moderator and the rotor. Such a correction to $\bar{l}_1$ can be written as a function of t' as

$$g(t') = \frac{\bar{l}_1(t') - \bar{l}_1}{\sin\alpha} = \begin{cases} c_1 + m_2(t' - \Gamma_2), & \text{for} \quad \Gamma_1 < t' < \Gamma_2, \\ m_1 t', & \text{for} \quad |t'| \leq \Gamma_1, \\ -c_1 + m_2(t' + \Gamma_2), & \text{for} \quad -\Gamma_2 < t' < -\Gamma_1, \\ \text{undefined}, & \text{otherwise.} \end{cases} \tag{32}$$

where

$$m_1 = c_2/\Gamma_1, \tag{33a}$$

$$m_2 = \frac{c_1 - c_2}{\Gamma_2 - \Gamma_1}, \tag{33b}$$

$$c_1 = h, \tag{33c}$$

$$c_2 = (h - w_r). \tag{33d}$$

2.5. Collimator function

Consider a Soller slit collimator located at a short distance l_c downstream of the chopper with an acceptance angle of horizontal divergence, ϕ_c. The probability of the chopped neutron beam passing through the collimator can be written as

$$P(t') = \int_{-w_c}^{w_c} \mathrm{d}x \, \Lambda_c\left(\frac{g(t')\cos\alpha - x}{l_1 + l_c}\right), \tag{34}$$

where $2w_c$ is the width of the collimator window and Λ_c is the collimator window function defined as

$$\Lambda_c(z) = \left(1 - \frac{|z|}{\phi_c}\right)\Theta\left(1 - \frac{|z|}{\phi_c}\right). \tag{35}$$

Having defined the chopper and the collimator transmission probability, Λ_r and Λ_c, as a function of $t' \equiv t_1 - t_0$, we now identify the window function for the chopper–collimator system mentioned in eq. (8) as

$$W(t') = \Lambda_r(t') * P. \tag{36}$$

2.6. Detector efficiency

The efficiency of a BF_3 or ^3He detector can be written [4] as

$$\eta(E) = \nu\left[1 - \exp\left(-N\sigma_d\sqrt{25/E}\,\mu\right)\right], \tag{37}$$

where E is the neutron energy, N is the number density of converter nuclei (^{10}B or ^3He), σ_d is the cross section for the neutron-induced nuclear reaction for a neutron energy of 25 meV, μ is the penetration thickness at the detection point and ν is the fraction of captured neutrons that actually result in an output pulse from the detector. In the case of a low-efficiency ($\eta \sim 1 \times 10^{-4}$) BF_3 counter the efficiency is inversely proportional to the neutron speed and a neutron is detected with equal probability throughout the detector thickness. For a high pressure ^3He detector one must correct, depending on the neutron energy, for the mean flight path in the detector relative to the detector thickness as the probability of a neutron being detected in the front is higher than that in the back of a detector.

3. The IPNS chopper spectrometers

The IPNS high-resolution and low-resolution medium-energy chopper spectrometers (HRMECS and LRMECS) have been in routine operation for a variety of experimental programs since 1981. The design and the performance of these machines have been reported in an earlier paper [10]. Here we only present the important features and the parameters which are relevant to the resolution consideration. HRMECS is located on the H-3 beam line viewing the H moderator and LRMECS on the F-4 line viewing the F moderator. Prior to 1986 both H and F moderator were made of high density polyethylene and at about 50 °C during operation. The details of the target, moderator and reflector system have been given elsewhere [11]. In 1986 for the purpose of better pulse shape and wider neutron energy spectrum polyethylene was replaced by liquid methane maintained at a physical temperature of about 100 K for both the H and F moderators [17]. Table 1 summarizes the important parameters for these moderators.

Fig. 2 shows the neutron count rate distributions from the IPNS polyethylene and methane moderators as measured by a beam monitor with a counting efficiency inversely proportional to the neutron speed. Note the shift of the Maxwellian component to lower energy as expected for the liquid methane moderator. The solid lines were obtained by fitting the data to the spectral function of eq. (19), taking into account an energy-independent delayed neutron background and the detector efficiency. As for the source pulse-shape function, in the case of a polyethylene moderator, we used the parameters measured by Ikeda and Carpenter [14] using time-focused crystal diffraction techniques. (At energies different from the measured values the pulse-shape parameters were obtained by interpolation.) Since no measurement has yet been made on the IPNS liquid methane moderators, we determined the pulse-shape parameters by fitting the time-of-flight data of the beam monitors with the calculated spectra. As an example the calculated pulse shapes for incident neutrons at 60 meV from both moderators are shown in fig. 3. As will be shown later, the narrower pulse width from the methane moderator results in a significant improvement of the energy resolution.

A variety of Fermi choppers have been designed to select neutron energies from about 5 to 1000 meV. Table 2 lists the parameters for the six choppers which are currently in use at IPNS. They rotate at a typical angular frequency of 270 Hz (at the ninth harmonic frequency of the IPNS rapid cycling synchrotron (RCS)) and are synchronized with the RCS proton triggering frequency. All choppers are operational with measured duty cycles of over 99% and the phasing time uncertainty is maintained to be less than 1 μs. The details of the chopper drive and phasing systems have been given elsewhere [18]. The chopper slit package consists of multiple, curved, parallel-sided, vertical slots packed to a cross sectional area compatible with the dimensions of a neutron beam. The slats were made of thin layers of composite boron–aluminum sheets so as to achieve a large effective neutron removal cross section over a wide range of energy. The typical relative neutron transmission at the optimal energy of a chopper is about 75%.

Table 1
Parameters of the IPNS moderators

(a) Dimension		
Width	0.1 m	
Height	0.1 m	
Tilt angle (α)	$-18°$ for HRMECS,	18° for LRMECS (see fig. 1)

(b) Spectral parameters

	Polyethylene	Liquid methane
Physical temperature	~ 320 K	~ 100 K
Φ_{Th}/Φ_{epi}	3.23	1.763
E_T	38.96 meV	11.09 meV
E_{co}	178.4 meV	65.76 meV
E_{ref}	1000 meV	1000 meV
s	3.59	2.57
ξ	0	0.077

(c) Measured pulse-shape parameters of the polyethylene moderators

E [meV]	H-moderator (HRMECS)			F-moderator (LRMECS)		
	a [μs^{-1}]	b [μs^{-1}]	R	a [μs^{-1}]	b [μs^{-1}]	R
2.53	0.125	0.043	0.995	0.158	0.047	0.995
10.12	0.172	0.043	0.952	0.211	0.047	0.880
22.77	0.230	0.037	0.844	0.265	0.046	0.825
40.48				0.317	0.047	0 796
63.25	0.360	0.039	0.750	0.365	0.049	0.718
123.97	0.485	0.052	0.565	0.511	0.058	0.541
161.92	0.540	0.059	0.432	0.568	0.067	0.444
204.93	0.620	0.063	0.329	0.657	0.066	0.368
306.13				0.788	0.061	0.351
364.32	0.817	0.042	0.231	0.860	0.064	0.296
647.68	1.113		0.0			

Table 2
Details of IPNS rotors

(a) Operation parameters		
	HRMECS	LRMECS
Moderator–chopper distance	12.7146 m	6.1784 m
Chopper–sample distance	1.150 m	0.6587 m
Angular frequency	270.0 Hz	270.0 Hz

(b) Rotor parameters

	Rotors					
	10-3	50-2	160-2	250-3	500-2	500-3
Window width [cm]	7.62	5.08	5.08	7.62	5.08	7.62
height [cm]	10.16	10.16	10.16	10.16	10.16	10.16
Optimal energy [meV]	10.0	50.0	165.3	250.0	500.0	500.0
$2r$ [cm]	12.70	15.40	15.40	12.70	15.40	12.70
ρ [cm]	40.76	91.15	165.74	203.82	288.24	288.24
d [cm]	0.254	0.254	0.203	0.127	0.157	0.102
Optimal transmission	0.90	0.82	0.79	0.78	0.74	0.74

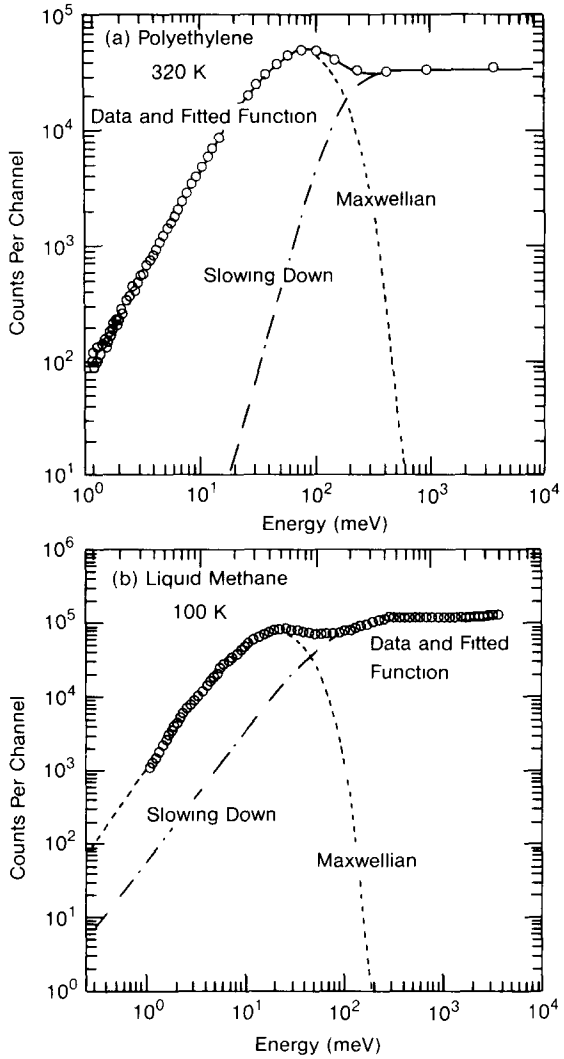

Fig. 2. The neutron count-rate distributions from the IPNS (a) polyethylene and (b) methane moderators as measured by a beam monitor with a counting efficiency inversely proportional to the neutron speed. The various lines represent the fitted spectral function, the Maxwellian and the slowing-down components.

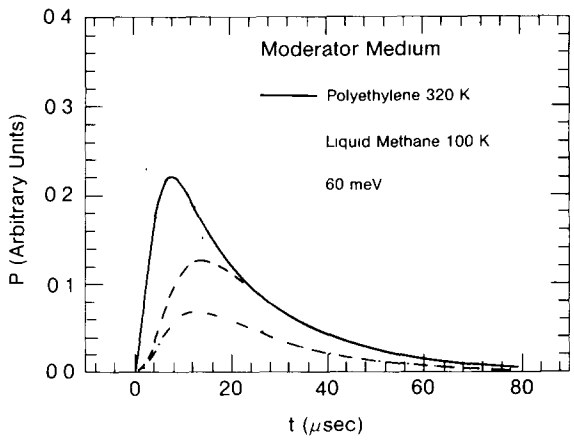

Fig. 3. The emission time distributions (pulse shapes) for a neutron energy of 60 meV emerging from the IPNS polyethylene (solid curve) and liquid methane (dotted curve) moderators. The pulse shape parameters are: polyethylene $a = 0.358$ μs^{-1}, $b = 0.049$ μs^{-1}, $R = 0.729$; liquid methane $a = 0.377$ μs^{-1}, $b = 0.052$ μs^{-1}, $R = 0.397$. The dashed and the dotted dashed curves correspond to the storage components for the polyethylene and the methane moderator respectively.

Table 3
Soller slit collimators of HRMECS and LRMECS

Collimator-sample distance	~ 0.65 m HRMECS ~ 0.35 m for LRMECS
Window width	7.75 cm
height	10.0 cm
Acceptance angle of horizontal divergence	40 min

The neutron beam transmitted through a chopper is reasonably collimated horizontally since the chopper also effectively acts as a rotating collimator. Nevertheless, it diverges at an angle comparable to the angle subtending the moderator face by the chopper aperture. To further refine the horizontal divergence of the incident beam, we have placed a Soller slit collimator with a horizontal acceptance angle of divergence of 40 minutes between the chopper and the sample. The collimator slits were made of thin plastic films coated with boron. The parameters of the collimators in use are listed in table 3.

As mentioned before in sect. 1, a pulsed-source chopper spectrometer enables measurements of inelastic scattering over a wide range of momentum and energy transfers. To realize this capability a final scattering flight-path chamber equipped with a large number of detectors at many scattering angles is indispensable. LRMECS has a detector bank covering angles from $-10°$ to $120°$. HRMECS presently has two scattering chambers: the low-angle one spans from $-20°$ to $20°$ and the high-angle one provides detector slots from $80°$ to $140°$. (We plan to install an intermediate-angle ($25°$ to $80°$) flight path in the near future.) The detectors are 6 atm ^{3}He proportional counters of 25 mm diameter. At large scattering angles the counters are 46 cm long but at small angles (therefore at low Q values) we use shorter tubes or linear position sensitive detectors to improve the Q resolution. We have also taken precaution to minimize, as much as possible, background scattering: the chambers are either in vacuum (LRMECS and HRMECS low-angles) or filled with inert gas at ambient pressure (HRMECS high-angle); in addition to the heavy shielding placed outside of the flight-path enclosures, the walls inside the scattering chambers are shielded by boron-containing materials against strayed neutrons. Details of the detector arrangements for HRMECS and LRMECS can be found in table 4.

The sample is enclosed in a high-vacuum chamber separated from the scattering flight path by thin aluminum windows. In normal situations, the sample is contained in an aluminum cell in the shape of either a thin slab or a cylinder. In the case of planar geometry, the slab is mounted at an angle (e.g. at $45°$) with the incident beam so that for all detector angles the beam traverses a mean path in the sample material comparable to the thickness of the plate. Such an arrangement minimizes multiple scattering of the neutrons by the sample. Background scattering can be assessed by measuring the empty container under identical conditions as in the sample run. The measurements of elastic incoherent scattering from

Table 4
Detector arrangements on HRMECS and LRMECS

(a) BF_3 fission chambers		
	HRMECS	LRMECS
Area	180.0 cm^2	180.0 cm^2
Thickness	3.7 cm	3.7 cm
Sample-detector distance		
Monitor 1	−0.8275 m	−0.4617 m
Monitor 2	5.1171 m	4.2932 m
(b) ^{3}He detectors		
	HRMECS	LRMECS
Tube diameter	2.54 cm	2 54 cm
Gas pressure	6 atm	6 atm
Scattering angles ($\bar{\phi}$)	$-20°$ to $20°$, $85°$ to $140°$	$-10°$ to $120°$
Increment of ϕ	0.3752°	0.6°
Length	10.64 cm for $\phi < 5°$ 45.72 cm for $\phi > 5°$	10.16 cm for $\phi \leq 3°$ 22.86 cm for $3° < \phi < 25°$ 45.72 cm for $\phi > 25°$
Sample–detector distance ($\bar{l}_3$)	~ 4.0 m	2.5 m
Detector–mid–plane distance ($\bar{z}$)	±0.227 m for $\phi > 5°$	0 m

vanadium provides detector calibration and intensity normalization to absolute units of the scattering cross section.

4. Results and discussion

Using a computer code for the resolution calculations as outlined in sect. 2 and the machine parameters of the IPNS chopper spectrometers in sect. 3, we now present the results of the calculation and compare them with the observed spectra. First, we discuss the intensity distribution of the incident neutrons, $I_0(v, t)$, sensed by a BF_3 beam monitor located at $\bar{l}$ downstream of the chopper in the forward direction. As an example, figs. 4a and 4b show the contour plots of the intensity distribution function, $I_0(v, t)$, calculated for neutrons with a mean incident energy of 146 meV at the LRMECS monitor 1 and monitor 2 positions respectively. Here we used the parameters corresponding to the IPNS ambient temperature polyethylene moderators, the 160-2 chopper and the LRMECS conventional configurations (see tables 1–4). We also assumed that the areas of the monitors are large enough to survey the entire beam. As expected, the intensity centers around $(\bar{v}_1, \bar{\tau})$, where $\bar{v}_1$ is the mean neutron speed given by eq. (13a) and $\bar{\tau}$ is the flight time at $\bar{l}$ for this speed given by $\bar{\tau} = \bar{l}/\bar{v}_1$. This point is represented by a cross in figs. 4a and 4b. On the other hand, $I_0(v, t)$ has an asymmetric shape which relates directly to the asymmetry of the source pulse shape. As given in eq. (21) and shown in fig. 3, the pulse shape function, characterized by the exponential time-decay constants a and b, in general extends to emission times considerably larger than the pulse widths. A chopper phased with the source selects neutrons of flight time $t_p + l_1/v$, as illustrated by the corresponding delta function in the integral of eq. (8). Thus more neutrons of higher speeds are selected by the chopper if there is a larger distribution of neutrons at longer t_p. As these neutrons travel along the flight path, their time of flight spreads according to the velocity distribution, and becomes larger at longer distance. This is clearly evident in the velocity distribution and the time-of-flight spectra shown in fig. 5. Fig. 5a shows the velocity distribution of the incident neutrons, $J_0(v)$, as obtained from eq. (12). The mean neutron speed, defined by eq. (13a), was found to be 5284.7 m/s (corresponding to a mean incident energy of 146.0 meV) whereas the peak was at 5252.2 m/s. Under normal experimental conditions, effects due to removal of neutrons by sample scattering and absorption are small, the shape of $J_0(v)$ remains unchanged at any position along the beam direction. The solid curves in figs. 5b and 5c represent the calculated time-of-flight intensity profiles for monitor 1 and monitor 2 respectively as given by eq. (10). Since the distance between the chopper and monitor 1 is short, the time spread by neutrons of different speeds is small. Therefore, the time-of-flight profile for monitor 1 is quite symmetric with respect to the mean arrival time (indicated by an arrow in the figure). As for monitor 2 (fig. 5c), the excess of neutrons of higher speeds arrives at shorter times resulting in a tail component on the left of the peak. In general, the shape of a monitor peak far away from the chopper resembles the source pulse shape but is reversed in time, analogous to the image of a distant object transmitted through a pinhole. In figs. 5b and 5c the circles represent the time-of-flight data measured by the monitors 1 and 2 of LRMECS which show excellent agreement with calculation. We also found excellent agreement between calculations and observed monitor peak shapes for both HRMECS and LRMECS at other energies between 30 and 1000 meV.

Next we consider scattering processes for neutron momentum and energy transfer $(\boldsymbol{Q}, E)$. In general this depends on the scattering function specific to the scatterer. Detailed calculations of the time-of-flight spectra and the resolution effects for specific problems will be given elsewhere [19]. Here we calculate the resolution function $R(\epsilon, t)$ from eq. (15b) by assuming a scattering function in the form of eq. (15a). Fig. 6 shows the results for LRMECS with $\bar{E}_1 = 146$ meV as in the above example at neutron energy transfers $\epsilon = -50$, 0, 50, and 100 meV. The detector is a 10.16 cm long ^{3}He tube centered at $-3.8°$ in the midplane ($z = 0$) of the spectrometer. The nominal E and Q resolution $(\Delta E, \Delta Q)$, in units of meV and Å^{-1}, can be obtained from eq. (18). They are (16.6, 0.059), (13.2, 0.045), (10.4, 0.038), and (8.4, 0.030) respectively for energy transfers of -50, 0, 50, and 100 meV. However, we emphasize that the resolution function cannot be approximated by a Gaussian function, as it can be seen in fig. 6 that the asymmetric line shapes prevail

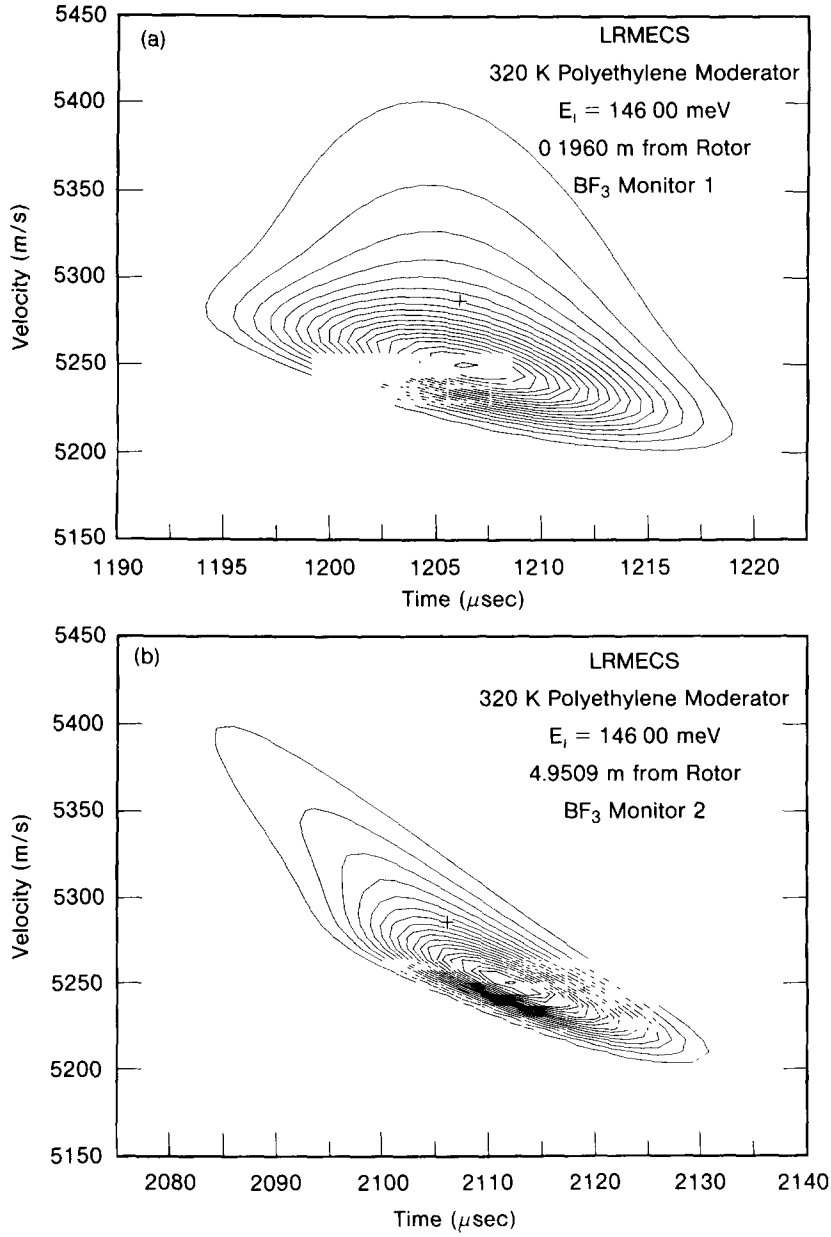

Fig. 4. Contour plots of the calculated intensity distribution functions for a mean neutron energy of 146 meV at the LRMECS monitor 1 and monitor 2 position.

at all energies. Therefore, in order to deduce quantitative information on $S(\boldsymbol{Q}, E)$ from the measured spectrum line shapes, one must take into account the detailed instrumental resolution as a function of momentum and energy transfer. The full width of $R(\epsilon, t)$ at half-maximum is in general smaller than the Gaussian equivalent width. Thus, a somewhat better nominal E resolution can be obtained if one uses the observed fwhm to define ΔE rather than eq. (18a). However, the fwhm is a quantity which is not easily amenable to analytical treatment.

At small scattering angles, the delta function of eq. (15a) is a good approximation for the scattering function of elastic incoherent scattering from a small piece of vanadium. Shown also in fig. 6d are the

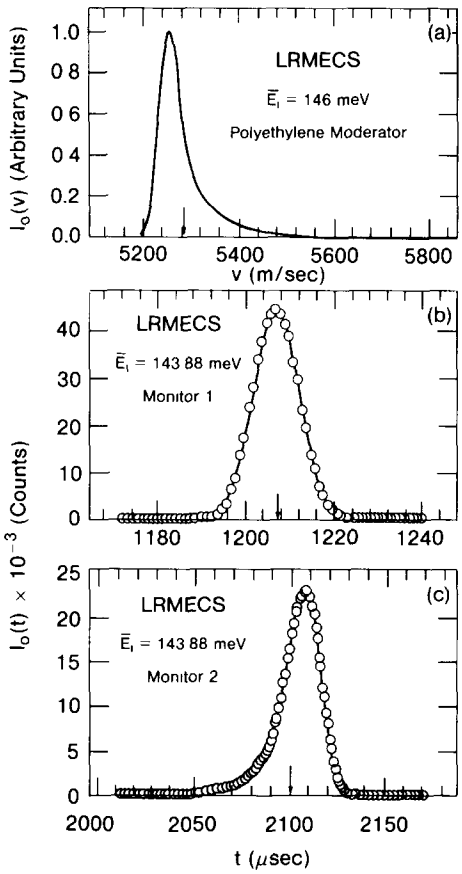

Fig. 5. (a) The calculated velocity distribution of incident neutrons at $\bar{E}_i = 146$ meV for LRMECS with the polyethylene moderator. (b), (c) The measured (circles) and the calculated (solid curves) intensity profiles of the LRMECS monitors. The mean incident energy was determined to be 143.88 meV.

observed time-of-flight data of a vanadium run. They agree well with the calculated spectrum. We also find similar good agreement in vanadium data for other neutron incident energies on both spectrometers. In the case of inelastic scattering, we use the magnetic scattering from a polycrystalline sample of $BaPrO_3$ as an example. At low temperature ($T = 20$ K) the crystal-field transition from the ground state to the first excited state in $BaPrO_3$ gives rise to an inelastic peak at about 252 meV. In a recent study [20], we found that the width of this peak is resolution limited and the intensity does not depend on the momentum transfer, apart from the magnetic form factor behavior of the Pr ions. Therefore, the scattering function can well be approximated by a delta function at the crystal-field splitting energy. Fig. 7 shows the comparison of the calculated and the observed spectrum. The data have been corrected for a smooth background mainly due to multiphonon and multiple scattering. The solid curve was obtained by fitting the data with a calculation corresponding to the HRMECS configurations including the sample and detector geometry. The agreement between data and calculation is very good. Therefore, our formulation of the resolution function for a pulse-source chopper spectrometer provides a satisfactory description of the incident and scattered time-of-flight spectra.

Bearing in mind that the resolution is not symmetric about a mean energy and momentum transfer, we present the nominal Q and E resolution for the IPNS chopper spectrometers as obtained from eq. (18). These results are useful as a general guideline in deciding the optimal configurations for an experiment. Table 5 lists the $\Delta E/E_i$ and $\Delta Q/Q$ of HRMECS at different scattering angles with an incident neutron energy of 150 meV. Liquid methane at about 100 K is used as the moderator medium and the 250-3 rotor

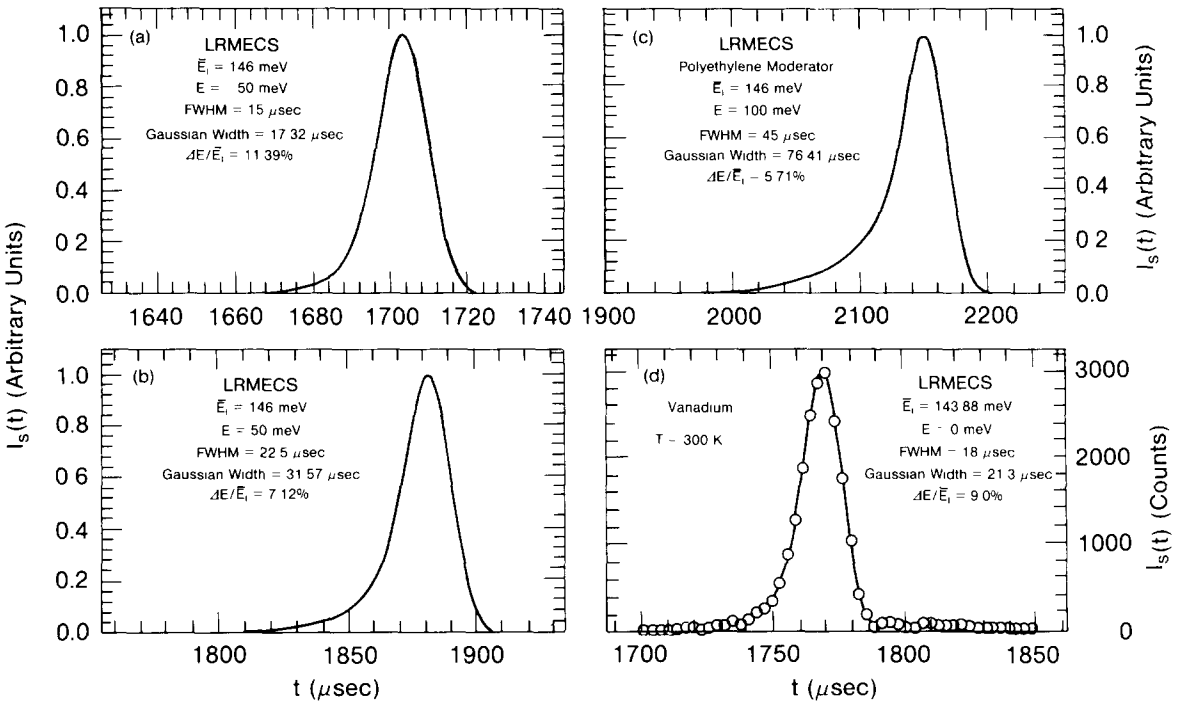

Fig. 6. (a)–(c) The calculated intensity profiles at energy transfers of −50, 50, and 100 meV for LRMECS with $\bar{E}_i = 146$ meV, polyethylene moderator and the 160-2 chopper. (d) The calculated spectrum (solid curve) at zero energy transfer and the measured data (circles) from vanadium at a scattering angle of −3.5°. The residual intensities on both sides of the elastic peak are due to phonon scattering.

is employed in this example. The detector at 3° is a 10.5 cm long element of a linear position sensitive ^{3}He detector and the others are 45.7 cm long tubes (see table 4). First, we point out that energy resolution becomes better as the neutron final energy decreases, which is in general true for an instrument designed

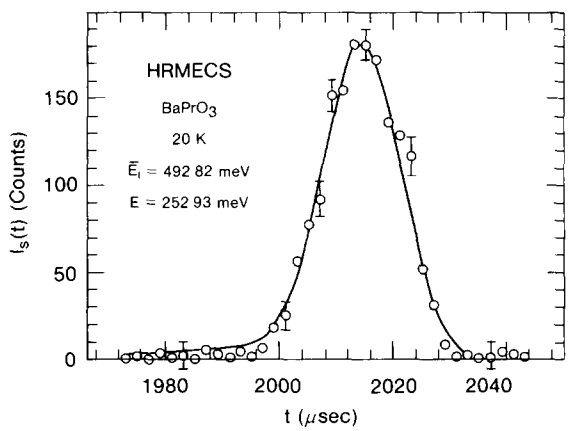

Fig. 7. The measured inelastic peak (circles) [20] corresponding to the crystal-field transition from the Γ_7 ground state to the Γ_8 excited state in $BaPrO_3$ as compared to the calculated spectrum (solid curve) (see text). The experiment was performed on HRMECS with the use of the polyethylene moderator and the 500-2 chopper. Neutron counts from six detector groups, each consisting of the four ^{3}He detectors, were added together and a smooth background level, representing multiphonon and multiple scattering, was subtracted from the data

Table 5
E and Q resolution of HRMECS with $\bar{E}_i = 150$ meV (liquid methane moderator, 250-3 chopper)

(a) E resolution							
	Energy transfer (E) in meV						
	−60	−30	0	30	60	90	120
$\Delta\bar{E}/\bar{E}_i$ [%]	5.7	5.0	4.4	3.8	3.3	2.9	2.4
(b) Q resolution							
	Scattering angles (ϕ) in degrees						
	3	3	15	60	90	120	160
Detector length [cm]	10.64	45.72	45.72	45.72	45.72	45.72	45.72
$E = -60$ meV							
$\bar{Q}$ [Å^{-1}]	1.71	1.71	2.92	9.39	13.18	16.10	18.29
$\Delta Q/\bar{Q}$ [%]	2.7	11.3	6.7	2.1	1.5	1.2	1.1
$E = -30$ meV							
$\bar{Q}$ [Å^{-1}]	1.06	1.06	2.51	8.95	12.62	15.44	17.55
$\Delta Q/\bar{Q}$ [%]	3.8	16.3	6.9	2.0	1.4	1.2	1.0
$E = 0$ meV							
$\bar{Q}$ [Å^{-1}]	0.66	0.66	2.27	8.52	12.03	14.73	16.75
$\Delta Q/\bar{Q}$ [%]	5.3	22.7	6.5	1.8	1.3	1.0	0.92
$E = 30$ meV							
$\bar{Q}$ [Å^{-1}]	1.09	1.09	2.33	8.10	11.42	13.96	15.87
$\Delta Q/\bar{Q}$ [%]	2.6	11.1	5.2	1.5	1.1	0.89	0.79
$E = 60$ meV							
$\bar{Q}$ [Å^{-1}]	2.00	2.00	2.77	7.74	10.76	13.11	14.87
$\Delta Q/\bar{Q}$ [%]	1.3	5.2	3.8	1.4	0.98	0.81	0.72
$E = 90$ meV							
$\bar{Q}$ [Å^{-1}]	3.16	3.16	3.61	7.46	10.07	12.13	13.68
$\Delta Q/\bar{Q}$ [%]	0.66	2.7	2.34	1.2	0.86	0.73	0.65
$E = 120$ meV							
$\bar{Q}$ [Å^{-1}]	4.71	4.71	4.94	7.39	9.32	10.92	12.15
$\Delta Q/\bar{Q}$ [%]	0.34	1.1	1.1	0.72	0.59	0.52	0.48

for direct geometry. Considering in addition the much sharper falloff on the right-hand side of the resolution function in the elastic region (see fig. 6) and the detailed balance factor in the scattering function, experimental conditions are much superior for scattering processes with neutron energy loss. Since a neutron cannot lose more energy than its incident energy, in conjunction with the requirement of low-Q data for many studies, high incident energy neutrons are required for measurements at large energy transfers. Here the advantage of a direct-geometry pulse-source machine is clear because of the availability of high fluxes of epithermal neutrons. Under the assumption of a Q-independent scatterer, the E resolution does not depend on Q. Second, consideration of Q resolution in the low Q-region requires the use of small or position sensitive detectors at small angles. For comparison we included in table 5 the Q resolution for using a 45 cm long detector at a scattering angle of 3°. The requirement for good Q resolution is more stringent in the case of single-crystal experiments since one aims at resolving information in the reduced wave vector $\boldsymbol{q}$ within the crystal Brillouin zone rather than in the neutron wave vector $\boldsymbol{a}$. Special precautions have to be taken in reducing the uncertainties due to sample and detector sizes as well as the beam (vertical) divergence.

The energy resolution in terms of $\Delta\bar{E}/\bar{E}_i$ for HRMECS and LRMECS under various conditions is shown in fig. 8. Although the calculations were done for a mean incident energy $E_i = 250$ meV using the 250-3 chopper, these results apply (within a 10% error) also to other energies with the use of the appropriate choppers. We note that in general a cold moderator provides better resolution because of the

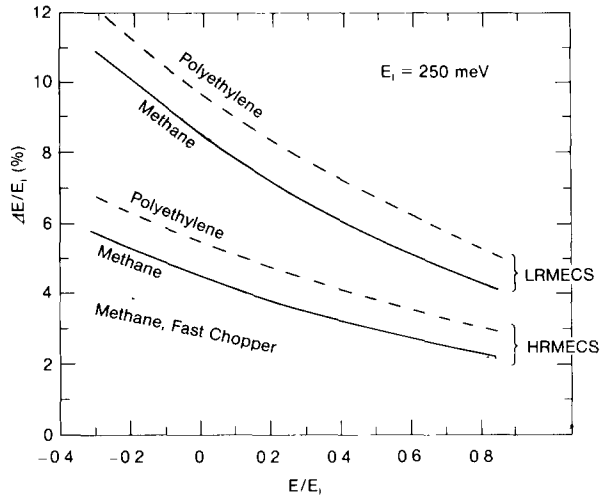

Fig. 8. The energy resolution in terms of $\Delta E/\bar{E}_i$ for HRMECS and LRMECS. The calculations were done for $\bar{E}_i = 250$ meV using the 250-3 rotor. The pulse-shape parameters are: polyethylene $a = 0.676\ \mu s^{-1}$, $b = 0.057\ \mu s^{-1}$, $R = 0.301$; methane $a = 0.585\ \mu s^{-1}$, $b = 0.085\ \mu s^{-1}$, $R = 0.255$. In the case of the fast chopper, the 250-3 rotor was assumed to have an angular frequency of 540 Hz with the slit curvature radius reduced to half of the present value.

suppression of the storage component in the source pulse. With the present liquid methane moderator, $\Delta E/E_i$ is about 2–4% and 6–8% for HRMECS and LRMECS respectively. This is in good agreement with those estimates [5] using the Gaussian approximation. As a reasonable compromise between intensity and resolution, the time uncertainties in the pulse emission and the chopper window function should match each other. At low incident energies ($E < 50$ meV), the pulse width is larger than the chopper width; therefore, the chopper slit width can be relaxed so as to increase neutron transmission. At high energies ($E > 150$ meV), on the other hand, the chopper scan time (the lighthouse effect) becomes the dominant factor in resolution consideration so it would be advantageous to increase the chopper angular speed or to narrow the collimation. As can be seen in fig. 8, the resolution would improve if the 250-3 chopper rotates at twice the present speed (540 Hz). The construction of a high-efficiency, high-speed chopper and drive system with a large aperture (~ 50 cm^2), however, is not a simple task. The design of such a chopper system is currently being studied at IPNS, as is the collimation option.

Now we address to the problem of energy-scale calibration for pulsed-source chopper spectrometers. Lacking the detailed information on the intensity distribution, the mean incident energy is determined as follows: Let the mean distance between monitor 1 (monitor 2) and the chopper be x_1 (x_2) and the mean arrival time of the monitor 1 (monitor 2) pulse defined by eq. (11) be τ_1 (τ_2). Then the observed incident neutron speed is given by

$$s_i = \frac{x}{\tau_2 - \tau_1}, \tag{38}$$

where $x \equiv x_2 - x_1$, and the mean flight time to the sample is taken to be

$$\tau_s = \tau_1 + \bar{l}_2/s_i. \tag{39}$$

For a given final flight time at the detector, t, the final speed of the neutrons is calculated from

$$s_f = \frac{\bar{l}_3}{t - \tau_s}. \tag{40}$$

Finally, the energy transfer as a function of time of flight is taken to be

$$\epsilon = \epsilon_i - \epsilon_f = \frac{m}{2}\left(s_i^2 - s_f^2\right). \tag{41}$$

As we shall show below, s_1 obtained by this method differs slightly from the mean incident speed, $\bar{v}_1$, defined by eq. (13) and the discrepancy depends on the extent of asymmetry in the monitor profiles. From eqs. (8) and (11),

$$\tau_2 = \int \mathrm{d}t_2\, t_2 \int \mathrm{d}v\, G(v,\, t_2 - x_2/v) = \int \mathrm{d}t_1\, (t_1 + x/v_0) \int \mathrm{d}v\, G(v,\, t_1 + x/v_0 - x_2/v)$$

$$= x/v_0 + \int \mathrm{d}t_1\, t_1 \int \mathrm{d}v\, G(v,\, t_1 + x/v_0 - x_2/v). \tag{42a}$$

Similarly,

$$\tau_1 = \int \mathrm{d}t_1\, t_1 \int \mathrm{d}v\, G(v,\, t_1 - x_1/v). \tag{42b}$$

Therefore,

$$v_0 = \frac{x}{\tau_2 - \tau_1 - \delta(v_0)}, \tag{43}$$

where

$$\delta(v_0) = \int \mathrm{d}t\, t \int \mathrm{d}v \left[G(v,\, t + x/v_0 - x_2/v) - G(v,\, t - x_1/v) \right]$$

$$= \int \mathrm{d}t\, t \left[I_0^{x_2}(t + x/v_0) - I_0^{x_1}(t) \right]. \tag{44}$$

Now let $v_0 = \bar{v}_1$; eq. (43) implies that if we intend to evaluate the mean incident speed $\bar{v}_1$ from the monitor times τ_1 and τ_2, a correction term, which in turn depends on $\bar{v}_1$, is required. As can be seen from eq. (44), $\delta(\bar{v}_1)$ is the mean time, averaged over the difference of the monitor 2 time-of-flight profile scaled back to the monitor 1 position by the mean speed $\bar{v}_1$ and the monitor 1 spectrum. In general this term is nonzero because of the asymmetric shapes of the monitor profiles. To further simplify this equation, first expand $G(v,\, t + x/v_0 - x_2/v)$ as

$$G(v,\, t + x/v_0 - x_2/v) = G(v,\, t - x_1/v + x/v_0 - x/v)$$

$$\simeq G\left(v,\, t - \frac{x_1}{v}\right) + x\left(\frac{1}{v_0} - \frac{1}{v}\right) \frac{\partial G(v,\, t - x_1/v)}{\partial t}, \tag{45}$$

then integrate over t by parts in eq. (42). We obtain, using eq. (13a),

$$\delta(v_0) \simeq -\int \mathrm{d}v\, x \left(\frac{1}{v_0} - \frac{1}{v}\right) \int \mathrm{d}t\, G\left(v,\, t - \frac{x_1}{v}\right) = x\left(\left[\frac{1}{v}\right] - \frac{1}{v_0}\right). \tag{46}$$

Therefore, as a first-order approximation, one may use

$$\delta(\bar{v}_1) \simeq x\left(\left[\frac{1}{v}\right] - \frac{1}{\bar{v}_1}\right). \tag{47}$$

We may then correct the mean incident neutron velocity and the time at sample as follows:

$$\bar{v}_1 = \frac{x}{\tau_2 - \tau_1 - \delta(\bar{v}_1)} \simeq s_1 \left(1 + \frac{\delta(\bar{v}_1)}{\tau_2 - \tau_1}\right), \tag{48}$$

$$\bar{t}_s = \tau_1 + l_2/\bar{v}_1 \simeq \tau_s + \frac{\bar{l}_2}{x}\delta(\bar{v}_1). \tag{49}$$

Table 6
Mean incident energy calibration of chopper spectrometers

Exp. conditions [a]	ϵ_1 [meV]	$\bar{E}_1$ [meV]	$\epsilon_{1,\mathrm{corr}}$ [meV]	$(\epsilon_1 - \bar{E}_1)/\bar{E}_1$ [%]
H, M, 50-2	35.10	34.75 ± 0.01	34.74	1.0
H, P, 50-2	50.17	49.44 ± 0.01	49.44	1.5
L. M, 50-2	60.70	59.70 ± 0.01	59.71	1.7
L, M. 160-2	120.92	119.18 ± 0.02	119.19	1 5
L, P, 160-2	147.08	143.88 ± 0.01	143.91	2.2
H, M, 160-2	150.62	149.49 ± 0.02	149.49	0.76
L, M, 160-2	160.34	157.73 ± 0.02	157.75	1.7
L, M, 250-2	254.90	249.98 ± 0.02	250.23	2.0
L, P, 160-2	298.90	294.07 ± 0.05	294.21	1.6
H, M, 500-3	347.27	344.36 ± 0.04	344.42	0.85
H, M, 500-3	496.45	490.73 ± 0.05	490.98	1.2
H, P, 500-2	497.22	492.82 ± 0.05	492.78	0.89
L, M, 500-3	500.67	490.49 ± 0.17	490.63	2.1
L, P, 500-2	765.15	753.40 ± 0.24	754.82	1 6
H, M, 500-3	792.32	781.57 ± 0.11	782.29	1.4
H, P, 500-2	796.96	787.23 ± 0.19	788.61	1 2
H, M, 500-3	1528.83	1504.74 ± 0.51	1507.32	1.6

[a] Spectrometer, moderator, and rotor: L = LRMECS, H = HRMECS; M = liquid methane, P = polyethylene.

In practice we have to fit the observed monitor 1 and monitor 2 spectra to the theoretical expression, $I_0(t)$ of eq. (10), by a least-squares analysis and thereby obtain $\bar{v}_1$ and $\delta(\bar{v}_1)$ from eqs. (13a) and (46) respectively. Since statistics of the monitor data are usually good, the mean incident energy, $\bar{E}_1$, can be determined very accurately as a parameter from the fit. An energy-transfer scale is then obtained from eqs. (40) and (41), with τ_s and ϵ_1 replaced by $\bar{t}_s$ and $\bar{E}_1$ respectively. In table 6 we give the results of the incident energy calibration for both chopper spectrometers. The data were obtained under configurations employing different moderators and choppers and transmitting neutrons over a wide range of energies. We find that in all cases the monitor spectra can be fitted well by the aforementioned theoretical expression. Furthermore, when one uses only the mean monitor times to find the incident energy, as described by eqs. (38)–(41), the obtained ϵ_1 is an overestimation of $\bar{E}_1$ by an amount of ~ 1–2% of $\bar{E}_1$. With the introduction of a correction term to the incident speed (see eq. (48)), the resulting energy, $\epsilon_{1,\mathrm{corr}}$, then agrees well with the $\bar{E}_1$ obtained from the fit. Therefore, these results demonstrate the self-consistency of this method for energy calibration. To give further credence to the conversion of time-of-flight scale to energy-transfer units, we plot in fig. 9 the measured scattering function of polycrystalline H_2O ice [21] at 20 K in the energy-transfer scales with and without the corrections for the incident energy and the time at sample. Clearly, the corrected energy spectrum shows an elastic peak centered at zero energy transfer, and the frequencies corresponding to the libration, the bond bending and stretching modes agree well with results from Raman scattering [22] and infrared absorption [23], contrary to the discrepancies shown in the uncorrected energy scale.

In summary, we have provided the analytical functions for the description of the performance of various components of a pulsed-source chopper spectrometer. Incorporating these functions into the detailed time and energy structure of the primary neutron source we have introduced a formulation for the evaluation of the transmitted neutron intensity distribution as a function of velocity and time. The convolution integral of a scattering function with the instrumental resolution for the scattered intensity as a function of neutron time of flight sensed by a detector was then given. To demonstrate the application of this theory, we compared extensively the results of the calculations with data taken by the two IPNS chopper spectrometers under many different experimental conditions. Excellent agreement was found between the detailed shapes of the intensity profiles between the observed monitor data and calculation. The resolution function at (Q, E), in terms of the scattering from a Q-independent scatterer at a resonant energy E, was calculated and the results were compared to the elastic incoherent scattering from vanadium

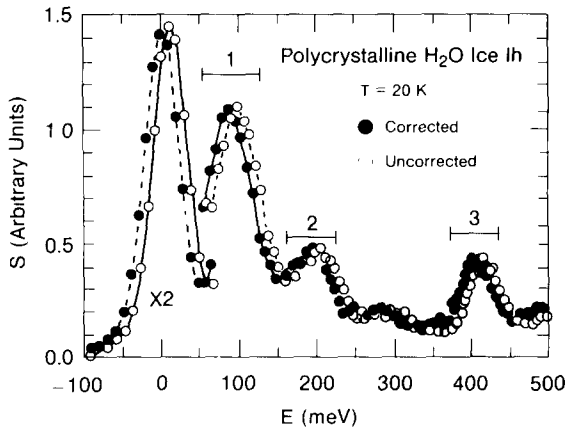

Fig. 9. The energy spectrum of polycrystalline H_2O ice in ref. [21] at 20 K measured on HRMECS with an incident energy of 788 meV. The open and closed circles represent the data plotted on the uncorrected and the corrected energy-transfer scales respectively (see text). The energy interval labels 1, 2 and 3 represent, respectively, the energy bands of the libration, the bond bending and bond stretching modes determined from Raman scattering [22] and infrared absorption [23] measurements.

and the spectrum of crystal-field transition in $PrBaO_3$. From least-squares analysis and hypothesis testing of the observed data and an assumed scattering function this formulation also provides a means for the determination of the scattering function from measured spectra. The Gaussian-equivalent Q and E resolution for the IPNS chopper spectrometers, and the possibilities of further improvements in resolution of pulsed-source instruments were discussed. Finally, we presented a method for the determination of the mean incident neutron energy and for the establishment of an energy-transfer scale in pulsed-source chopper experiments.

Acknowledgements

We are indebted to Drs. D.L. Price, P.E. Sokol, M. Arai, R.K. Crawford, R.O. Simmons, R.N. Sinclair, C.G. Windsor, and A.D. Taylor for many helpful suggestions. The chopper control tests conducted by Mr. G.E. Ostrowski in the course of our studies are gratefully acknowledged. One of us (C.K.L.) wishes to thank the Booster Synchrotron Facility of the National Laboratory for High Energy Physics of Japan for the hospitality and the support during his visit in which the intermediate analysis of this work was carried out. IPNS is supported by the US Department of Energy, Basic Energy Sciences, Division of Materials Science.

References

[1] R.J. Royston, Nucl. Instr. and Meth. 30 (1964) 184.
[2] H. Bjerrum Møller and M. Nielsen, in: Instrumentation for Neutron Inelastic Scattering Research (IAEA, Vienna, 1970) p. 49.
[3] S. Komura and M.J. Cooper, Jap. J. Appl. Phys. 9 (1970) 866.
[4] J.M. Carpenter, D.L. Price and N.J. Swanson, Argonne National Laboratory, Report ANL-78-88 (1978).
[5] D.L. Price and S.K. Sinha, private communication.
[6] C.L. Carlile, A.D. Taylor and W.G. Williams, Rutherford Appleton Laboratory, Report RAL-85-052 (1985).
[7] M. Marseguerra and G. Pauli, Nucl. Instr. and Meth. 4 (1959) 140.
[8] J.R.D. Copley, Comp. Phys. Commun. 21 (1981) 431 and references therein.
[9] P.E. Sokol, D.L. Price and J.M. Carpenter, to be published.
[10] D.L. Price, J.M. Carpenter, C.A. Pelizzari, S.K. Sinha, I. Bresof and G.E. Ostrowski, Proc. 6th Meeting of the International Collaboration on Advanced Neutron Sources (ICANS VI, 1982) ANL-82-80 (1983) p. 207.
[11] J.M. Carpenter, S. Cudrnak and C.M. DeCusatis, Proc. 9th Meeting of the International Collaboration on Advanced Neutron Sources (ICANS-IX) (1986) to be published.

[12] J.M. Carpenter, M.H. Mueller, R.A. Beyerlein, T.G. Worlton, J.D. Jorgensen, T.O. Brun, K. Sköld, C.A. Pelizzari, S.W. Peterson, N. Watanabe, M. Kimura and J.E. Gunning, Proc. Neutron Diffraction Conf., Petten, The Netherlands, and F. Kropff, J.R. Granada and R.E. Mayer, Nucl. Instr. and Meth. 198 (1982) 515.
[13] J.M. Carpenter, R.A. Robinson, A.D. Taylor and D.J. Picton, Nucl. Instr. and Meth. A234 (1985) 542.
[14] S. Ikeda and J.M. Carpenter, Nucl. Instr. and Meth. A239 (1985) 536.
[15] J.M. Carpenter, private communication.
[16] J.M. Carpenter and C.A. Pelizzari, unpublished information (1978).
[17] J.M. Carpenter, A.W. Schulke, T.L. Scott, D.G. Wozniak, B.E. Benson and B.D. Leyda, Proc. 8th Meeting of the International Collaboration on Advanced Neutron Sources (ICAN-VIII) (1985) Rutherford Appleton Laboratory Report RAL-85-110, p. 311.
[18] G.E. Ostrowski, L.I. Donley, A.V. Rauchas, G.J. Volk, E.A. Jung, J.R. Haumann and C.A. Pelizzari, ibid., p. 676; and L.I. Donley, ibid, p. 689.
[19] P.E. Sokol, C.-K. Loong, D.L. Price and J.M. Carpenter, to be published.
[20] S. Kern, C.-K. Loong and G.H. Lander, Phys. Rev. B32 (1985) 3051.
[21] C. Andreani, P. Bosi, F. Sacchetti and C.-K. Loong, J. Chem. Phys. 83 (1985) 750.
[22] T.C. Sivakumar, S.A. Rice and M.G. Sceats, J. Chem. Phys. 69 (1978) 3468.
[23] J.E. Bertie and E. Whalley, J. Chem. Phys. 40 (1964) 1646.